Function and Cryo-EM structures of broadly potent bispecific antibodies against multiple SARS-CoV-2 Omicron sublineages

Ping Ren [1,2,3,*], Yingxia Hu [4,*], Lei Peng [1,2,3,*],
Luojia Yang [1,2,3,4], Kazushi Suzuki [1,2,3],
Zhenhao Fang [1,2,3], Meizhu Bai [1,2,3], Liqun Zhou [1,2,3,5], Yanzhi Feng [1,2,3,5],
Yong Xiong [4,@], and Sidi Chen [1,2,3,4,5,6,7,8,@]

Affiliations

1. Department of Genetics, Yale University School of Medicine, New Haven, CT, USA
2. System Biology Institute, Yale University, West Haven, CT, USA
3. Center for Cancer Systems Biology, Yale University, West Haven, CT, USA
4. Department of Molecular Biophysics and Biochemistry, Yale University, New Haven, CT, USA
5. Molecular Cell Biology, Genetics, and Development Program, Yale University, New Haven, CT, USA
6. Immunobiology Program, Yale University, New Haven, CT, USA
7. Comprehensive Cancer Center, Yale University School of Medicine, New Haven, CT, USA
8. Stem Cell Center, Yale University School of Medicine, New Haven, CT, USA
9. Center for Biomedical Data Science, Yale University School of Medicine, New Haven, CT, USA

* Co-first authors.

@ Correspondence:
SC (sidi.chen@yale.edu)
+1-203-737-3825 (office)
+1-203-737-4952 (lab)

YX (yong.xiong@yale.edu)
+1 (203) 436-2609 (lab)

Abstract

The SARS-CoV-2 variant, Omicron (B.1.1.529), rapidly swept the world since its emergence. Compared with previous variants, Omicron has a high number of mutations, especially those in its spike glycoprotein that drastically dampen or abolish the efficacy of currently available vaccines and therapeutic antibodies. Several major sublineages of Omicron involved, including BA.1, BA.2, BA.2.12.1, BA.3 and BA.4/BA.5, rapidly changing the global and regional landscape of the pandemic. Although vaccines are available, therapeutic antibodies remain critical for infected and especially hospitalized patients. To address this, we have designed and generated a panel of human/humanized therapeutic bispecific antibodies against Omicron and its sub-lineage variants, with activity spectrum against other lineages. Among these, the top clone CoV2-0213 has broadly potent activities against multiple SARS-CoV-2 ancestral and Omicron lineages, including BA.1, BA.1.1, BA.2, BA.2.12.1, BA.3 and BA.4/BA.5. We have solved the cryo-EM structure of the lead bi-specific antibody CoV-0213 and its major Fab arm MB.02. Three-dimensional structural analysis shows distinct epitope of antibody – spike receptor binding domain (RBD) interactions, and demonstrates that both Fab fragments of the same molecule of CoV2-0213 can target the same spike trimer simultaneously, further corroborating its mechanism of action. CoV2-0213 represents a unique and potent broad-spectrum SARS-CoV-2 neutralizing bispecific antibody (nbsAb) against the currently circulating major Omicron variants (BA.1, BA.1.1, BA.2, BA.2.12.1, BA.3 and BA.4/BA.5), while maintaining activity against certain ancestral lineages (WT/WA-1, Delta), and to some degree other β-coronavirus species (SARS-CoV). CoV2-0213 is primarily human and ready for translational testing as a countermeasure against the ever-evolving pathogen.

Key words

Bispecific antibody, nbsAb, SARS-CoV-2, WA1, Delta, Omicron (B.1.1.529), BA.1, BA.2, BA.3, BA.2.12.1, BA.4/BA.5, neutralization, Cryo-EM structure

The SARS-CoV-2 pathogen rapidly disseminates globally, with constantly evolving landscape in the pandemic [1]. To date, the COVID-19 pandemic has infected nearly 600 million confirmed individuals and caused over 6.4 million deaths (https://www.worldometers.info/coronavirus/). One of the most concerning features of the virus is that the pathogen SARS-CoV-2 continues to evolve. Numerous mutant lineages emerged, some became dominant while some diminished, leading to multiple waves across the world (**Fig. 1A**). The Omicron variant (B.1.1.529), initially reported in South Africa in late 2021, rapidly became the predominant variant circulating in many countries and led the fourth pandemic wave globally [2]. As compared with the genome sequences of ancestral variants of concerns (VOCs), the Omicron lineage has harbored a high number of genomic mutations, especially in the spike (S) glycoprotein and clustered in the receptor-binding domain (RBD) (**Fig. 1B**). These mutations drastically decrease the efficacy of currently available vaccines and FDA-approved or emergency use authorized (EUA) monoclonal antibody-based therapies [2-8] (Table. S1).

As of today, the original Omicron lineage has evolved multiple distinct sub-lineages, such as BA.1, BA.2, BA.3, and BA.4/BA.5 according to WHO weekly epidemiological update[9-11]. BA.1.1 (a subvariant of BA.1) has an additional R346K mutation and caused large regional outbreaks in Canada with BA.1 during the first quarter of 2022[12]. BA.2.12.1 (a subvariant of BA.2), which carried two additional alterations (L452 and S704) on top of BA.2 (**Fig. 1C**), has emerged and once become the dominant variant in the US and certain other regions [13]. In addition, BA.4/BA.5, which shared identical sequence of the spike protein, contained additional mutations (Del69-70, L452R, F486V and R493Q) compared to BA.2 (**Fig. 1C**), and become dominant in several major regions of the world, including US and China [14]. These phenomena indicate rapid dynamics of the viral evolution, leading to substantial changes in infectivity, antigenic escape, reduction of vaccine efficacy, and increased possibility of repeat infections[3,8,13,15,16]. Although vaccines are available, therapeutic antibodies remain critical for infected and especially hospitalized patients. However, few clinical monoclonal antibodies can retain substantial activities against all Omicron sublineages [13], urging for more and therapeutic options[14,17]. Therefore, it is critical to rapidly develop countermeasures such as new antibodies against these sublineages.

We therefore set out to develop new candidates of monoclonal therapeutic antibodies that can counter multiple Omicron sub-lineages. We first examined the Omicron RBD-directed neutralizing monoclonal antibodies (MB.02, MB.08, PC.03) [18]. Results showed that while all three mAbs strongly bind Omicron

BA.1 RBD, two of these three mAbs exhibited reduced binding activity against Omicron BA.2 (**Fig. 1D**). Yet, one of these mAbs, MB.02, maintains high level of binding against BA.2 (0.003 μg/mL, low single digit ng/mL EC50) (**Fig. 1D**, lower panel).

To avoid potential immune escape and infection by SARS-CoV-2 mutational variants, cocktail strategies (i.e., administration of two human monoclonal antibodies) were previously designed and reported, which had been demonstrated that could largely increase efficacy and maximally prevent viral escape [19-21]. However, cocktail strategy requires production of multiple molecules. On the contrary, bispecific antibody (bsAb) strategy can simultaneously target two different antigens or antigenic sites according to its structural design. In addition, bsAb can benefit from synergistic effects of the two binder Fab arms [22]. An effective dual-binder bsAb can also save the manufacturing process cost by half as compared to a cocktail of two mono-specific mAbs, which can be substantial in translational and clinical stage development. Furthermore, the dual-targeting concept has already been successfully studied as an effective strategy in treatment of cancer and inflammatory disorders [23-25]. In addition, several studies have been illustrated that bispecific antibodies could potently enhance breadth and potency than parental monoclonal antibodies [26-28].

Due to extensive mutations in the spike protein, Omicron sublineages are drastically different from the variants in the ancestral lineages (e.g., wildtype, WT, Wuhan-1, WA-1) and earlier variants (such as Delta variant, B.1.617.2). To develop potential broad spectrum SARS-COV-2-specific functional bispecific antibodies, we engineered five bispecific antibodies in this study by using an IgG1 knob-into-hole bispecific CrossMab antibody technique (**Fig. 2A**), utilizing the Fab regions from four of our previously developed fully human or largely humanized monoclonal antibodies, Clones MB.02, MB.08, PC.03[18] and Clone 13A[29]. The resultant bsAb clones were named as CoV2-0208, CoV2-0203, CoV2-0803, CoV2-0213 and CoV2-0813, respectively, based on the compositions of their respective parental monospecific mAb clones. To determine the purity of those bispecific antibodies, we analyzed the molecular weight of separated modules by using reduced SDS-PAGE after Protein A beads purification. The findings indicated that all our bispecific antibodies are successfully expressed with expected size with high purity after protein A purification (**Fig. 2B**).

To identify the binding properties of the five purified bispecific antibodies, we performed antibody titration assays by ELISA with four SARS-CoV-2 RBD recombinant proteins, which included SARS-CoV-2-WA-1 RBD, SARS-CoV-2-Delta RBD, SARS-CoV-2-Omicron BA.1 RBD and SARS-CoV-2-Omicron BA.2 RBD (**Fig. 2C**). We included the clinically relevant mAb S309 (Sotrovimab) in the experiment, which has been in human use under Food and Drug Administration (FDA) issued emergency use authorization (EUA) in the US, and similarly in Europe, UK, Japan and Australia. Among the bsAbs, only CoV2-0213 and CoV2-0813 exhibited substantially lower half-maximum effective concentration (EC_{50}) value to all four SARS-CoV-2-RBDs, similar to S309 (**Fig. 2D**). The remaining bsAbs only showed substantially lower EC_{50}(s) to one or two of SARS-CoV-2-RBD(s) (**Fig. 2C**). Meanwhile, our lead bsAbs, CoV2-0213 and CoV2-0813, also exhibited strong competition with angiotensin-converting enzyme 2 (ACE2) for binding to a range of SARS-CoV-2 RBDs (**Fig. S1**).

To further assess the functional properties of the five bispecific antibodies in vitro, we first performed neutralization assay with HIV-1 based pseudoviruses (**Fig. S2**), a widely used assay by the field [30-33]. As observed, mAb S309 retained neutralization activity against both Omicron BA.1 and BA.1.1 (BA.1+R346 mutation) with half-maximum inhibitory concentration (IC_{50}) values of 0.44 and 0.53 μg/mL, respectively. However, its neutralization activity against Omicron BA.2 dropped 30-fold to an IC_{50} value of 2.75μg/mL (**Fig. 3A**). Of note, the EUA of S309/Sotrovimab was recently withdrawn by FDA in March 2022 due to the high prevalence of BA.2 variant in many states in the US. In contrast, one of our lead bispecific antibodies, CoV2-0213, displayed broad spectrum neutralization ability to a range of SARS-CoV-2 VOCs (**Fig. 3A**). Specifically, CoV2-0213 remained potent in neutralizing three of Omicron sublineages, BA.1, BA.1.1 and BA.2, with IC_{50} values of 0.044, 0,062 and 0.078 μg/mL, respectively (**Fig. 3B**). The bsAb CoV2-0213 is an order-of-magnitude more potent than S309/Sotrovimab in neutralization against BA.1 and BA.1.1, and ~78x more potent than S309/Sotrovimab against BA.2. Meanwhile, two other bispecific antibodies also exhibit potent Omicron-specific neutralization. CoV2-0203 showed high potency in neutralizing the three of Omicron sublineages, although it showed relatively weak neutralization ability (1.5-fold weaker) in comparison to CoV2-0213 (**Fig. 3B**). CoV2-0208 showed high potency against BA.1 and BA.1.1, but its activity against BA.2 is on par with S309 (**Fig. 3B**). Both CoV2-0208 and CoV2-0203 lost neutralization activity against the Delta variant. Thus, our lead bsAb is CoV2-0213, which has strong neutralization potency against Omicron BA.1, BA.1.1 and BA.2 and maintains reasonable activity against Delta. Subsequently, we evaluated the binding affinity of CoV2-0213 with three Omicron subvariants including Omicron BA.1, BA.1.1, and BA.2 RBD proteins by biolayer interferometry (BLI). The BLI results revealed that the lead bispecific antibody, CoV2-0213, indeed displays high single molecule affinity, at single-digit nanomolar Kd against Omicron BA.1 (Kd = 2.9 nM) and BA.2 (Kd = 6.98 nM) (**Fig. 3C**).

To better understand the mechanism of action of the bsAb CoV-0213, we performed cryo-electron microscopy (cryo-EM) studies to solve the three-dimensional (3D) structures of the bsAb and its major Fab arm (MB.02) in complexes with the Omicron spike variants (we previously reported the cryo-EM structure of the other Fab arm, 13A in complex with WT spike[29]). We first sought to map the molecular basis for the broad specificity of MB.02 and its interaction with the RBD epitope, and determined the cryo-EM structures of MB.02 Fab in complex with the ectodomain of Omicron BA.1 spike trimer (S trimer) at ~3.2 Å resolution (**Table 1**). Two major S trimer conformation states were detected, one with one RBD up (72%) and the other with two RBDs up (28%) (**Fig. 4A**). In both conformations, the S trimer is bound with three Fab molecules, one per RBD. The binding of MB.02 Fab makes the spike RBD more flexible, especially in up conformation (**Fig. S3A**). MB.02 Fab mainly contacts a flexible loop region at the left shoulder region of spike RBD. The MB.02 Fab-binding interface on spike RBD has no overlap with the ACE2-binding interface, although there could be slight steric clashes between the bound ACE2 and MB.02 (**Fig. 4B**). All six complementarity determining regions (CDRs) of the MB.02 Fab participate in RBD interactions (**Fig. 4C**). The omicron BA.1 spike RBD maintains an overall architecture similar to that of the WT spike from the ancestorial lineage, with minor local conformational changes primarily at the mutation sites. The MB.02-binding interface contains two mutations (N440K and G446S), with N440K contacting CDRH1 and CDRH2 of MB.02, and G446S interacting with the CDRL2 loop (**Fig. 4C**, lower panel).

To further evaluate cross-reactivity of CoV2-0213 against other SARS-CoV-2 variants and coronavirus species, we performed antibody titration assays by ELISA with six additional human coronaviruses RBD proteins, which included four Omicron sublineages (BA.2, BA.2.12.1, BA.3 and BA.4/BA.5) and two β-coronaviruses (SARS-CoV and MERS-CoV). The results showed that CoV2-0213 has broad binding activity to all assayed RBDs of Omicron sublineages BA.2, BA.2.12.1, BA.3 and BA.4/BA.5, with EC_{50} values ranging from 0.004 to 0.016 µg/mL, with weak to moderate cross-reactivity to SARS-CoV and MERS-CoV RBD proteins (**Fig. 5A**). Subsequently, we measured binding affinity of CoV2-

0213 with three additional Omicron subvariants including Omicron BA.2.12.1, BA.3 and BA.4/BA.5 RBD proteins by the BLI, and used Omicron BA.2 RBD protein as positive control. The BLI results revealed that the lead bispecific antibody, CoV2-0213, retains high affinity with low nanomolar Kd against Omicron BA.2.12.1 (Kd = 13.4 nM), BA.3 (Kd = 4.6 nM) and BA.4/5 (Kd = 44.4 nM) RBD, respectively (**Fig. 5B**). We analyzed the RBD mutations in BA.2.12.1, BA.3 and BA.4/5 that are directly located at the CoV2-0213 binding interface. The mutation G446S that could be important for MB.02 binding (**Fig. 4C & Fig. 6A**), is present in BA.3 but not in BA.2.12.1 and BA.4/5, while F486V that may disrupt the Clone 13A interaction, is present in BA.4/5 only (**Fig. 6A**). These differences may explain the enhanced binding affinity of CoV2-0213 bsAb to different Omicron subvariants, although other spike RBD mutations may also have indirect allosteric effects on the RBD conformation at the CoV2-0213 binding interface.

The lead bispecific antibody, CoV2-0213, exhibited significant or even enhanced binding affinity and neutralizing efficacy to a wide range of assayed Omicron subvariants compared to its parental monoclonal antibodies[18], suggesting its promise as a potent and more cost-effective candidate as compared to using two single mAbs. One Fab arm of CoV2-0213, Clone 13A, the humanized clone 2 antibody for WT spike [22], mainly interacts with the right ridge of spike RBD and would not lead to any steric clash with a bound MB.02, suggesting they could target the same RBD simuntaniously (**Fig. 6A**). To further investigate how CoV2-0213 bsAb binds to the spike antigen, we determined the cryo-EM structure of CoV2-0213 bsAb in complex with the recently emerged and prevalent BA.5 Omicron subvariant. Of note, it has been challenging to solve a Cryo-EM structure of a bispecific IgG with two arms bound to SARS-CoV-2 spike, where none of the previous COVID bispecific antibody studies report such a IgG structure. This is due to potential steric hinderance or instability of two simultaneously bound Fab arms, a major challenge in designing effective bispecific antibodies. We overcame this challenge, and solve the cryo-EM structure of CoV2-0213 with both Fab arms fully engaged to the spiker trimer.

Among the cryo-EM particles we collected, only one spike conformation with one RBD up was detected (**Fig. 6B**). From that, we further identified a subset (~24%) of particles with density for two Fab fragments on the same RBD in the up conformation, and one Fab fragment each for the other two RBDs in the down conformation (**Fig. 6B, left panel**). The density for the Fab-bound up-RBD fitted well with the overlaid model of spike RBD with the MB.02 and Clone 13A Fab fragments[29], while the density of the Fab-bound down RBDs matched with the model of the MB.02 Fab-bound RBD (**Fig. 6B, right panel**). This means that we detected three MB.02 and one Clone 13A Fabs bound to the same S trimer, potentially from three 0213 bsAbs with one of them having both Fab arms bound. The flexible Fc region could not be visualized in the cryo-EM reconstruction and thefore we could not identify which bound MB.02 Fab and Clone 13A Fab were from the same CoV2-0213 bsAb. Considering the flexible nature of the hinge region of an IgG, it is possible that the two Fab arms of a CoV2-0213 bsAb can target one single spike RBD or two adjcent ones in the same trimer simuntaniously (**Fig. 6C**). It is also possible the observed four bound-Fab fragments are from four different CoV2-0213 bsAbs. Regardless of which mode the bsAb binds to the spike RBD, our observation provides a 3D structure view of explanation for the enhanced engagement of Omicron spike and neutraliztion effect by CoV2-0213.

In summary, we have generated five distinct SARS-CoV-2-targeting nbsAbs and evaluated their functional properties against the ancestral and Omicron (sub)lineages. Our lead nbsAb, CoV2-0213, exhibited potent and broad-spectrum activities ability to a range of SARS-CoV-2 VoCs, including all major Omicron sublineages (BA.1, BA.1.1, BA.2, BA.2.12.1, BA.3 and BA.4/BA.5), certain ancestral lineages (WT/WA-1, Delta), and to some degree other β-coronavirus species (SARS-CoV). Our cryo-EM structure demonstrated that the two Fabs arms of CoV2-0213 can fully engage the same SARS-CoV-2 spiker trimer simultaneously. CoV2-0213 is primarily human and ready for translational testing as a countermeasure against the ever-evolving pathogen.

Acknowledgments

We thank various members from our labs for discussions and support. We thank staffs from various Yale core facilities for technical support. We thank all staffs at the Laboratory for BioMolecular Structure (LBMS) at Brookhaven National Lab for support in cryo-EM data collection. We thank Drs. D Klein, L Chen, M Müschen and others for providing equipment and related support. We thank various support from Department of Genetics; Institutes of Systems Biology and Cancer Biology; Dean's Office of Yale School of Medicine and the Office of Vice Provost for Research.

Funding

This work is supported by DoD PRMRP IIAR (W81XWH-21-1-0019) and discretionary funds to SC and NIH R01AI163395 to YX. The LBMS is supported by the DOE Office of Biological and Environmental Research (KP1607011).

Institutional Approval

All recombinant DNA (rDNA) and biosafety work were performed under the guidelines of Yale Environment, Health and Safety (EHS) Committee with approved protocols (Chen 15-45, 18-45, 20-18, 20-26).

Author Contributions

PR: design of the bispecific antibodies, construct generation, cloning, antibody expression, ELISA, data analysis, figure prep, writing

YH: Cryo-EM, structure studies, writing

LP: construct generation, cloning, neutralization, data analysis, figure prep

LY, KS, MB, YF: assisting experiments and data collection

ZF, LZ: construct generation, cloning, resources

YX: Cryo-EM, structure studies, funding, supervision, writing

SC: conceptualization, overall design, funding, supervision, writing

Methods

Cloning and expression of SARS-CoV2-specific human bispecific antibodies

Bispecific antibodies were cloned and expressed as previously described [29]. In brief, indicated mAb variable regions for each bispecific antibody were amplified and subcloned into separate mammalian expression vectors using Gibson assembly [29]. To express recombinant bispecific antibodies, four expression vectors were transiently transfected into Expi293 cells using ExpiFectamine 293 transfection kit according to the manufacturer's protocol (ThermoFisher). Antibody containing cell culture supernatants were harvested after 5 days of cultivation in shake flasks, then secreted bispecific antibodies were collected and purified by affinity chromatography using rProtein A Sepharose Fast Flow beads (Cytiva, Cat: #17127901). Purified bispecific antibodies were inspected using SDS-PAGE and stored at -80°C after further usage.

SARS-CoV-2 pseudovirus generation and neutralization assay

The SARS-CoV-2 pseudovirus was produced as previously described [18]. Briefly, pseudovirus containing cell culture supernatant was harvested after 2 days of co-transfection of HEK-293T cells with a spike-expressing plasmid and env-deficient HIV-1 backbone vectors, then clarified by centrifugation and stored at -80°C after further usage. To determine the neutralizing activity of bispecific antibody, serial diluted antibodies were incubated with pseudovirus at 37°C for 1hour, then co-cultured with HEK-293T-hACE2 cells for overnight. Finally, signal was evaluated after 24 hours by detection of GFP expression in the HEK-293T-hACE2 cells using Attune NxT Acoustic Focusing Cytometer (ThermoFisher) or BD Symphony Flow Cytromety.

Antibody binding quantification and ACE2 competition assay

The binding of bispecific antibodies were quantified by ELISA and ACE2 competition assays, as previously described [18]. The recombinant SARS-CoV-2 RBD wild type (WA-1) (Cat. No. 40592-V08B), SARS-CoV-2 Delta RBD (Cat. No.40592-V08H90), SARS-CoV-2 Omicron BA.1 RBD (Cat. No.40592-V08H121), SARS-CoV-2 Omicron BA.2 RBD (Cat. No.SPD-C522G-100ug), SARS-CoV-2 Omicron BA.2.12.1 RBD (Cat. No. SPD-C522Q-100ug), SARS-CoV-2 Omicron BA.3 RBD (Cat. No. SPD-C522I-100ug), SARS-CoV-2 Omicron BA.4/BA.5 RBD (Cat. No. SPD-C522R-100ug) used in ELISA quantification were purchased from Sino Biological and AcroBiosystems, respectively[18]. The ACE2 (Cat. No.10108-H08H) used in ACE2 competition assay was purchased from Sino Biological [29].

Bispecific antibody binding affinity measurement

The binding affinity of antibodies with RBD was performed previously by Octet RED96e (ForteBio) using bio-layer interferometry (BLI). 25ng/µl of purified bispecific antibody was immobilized onto AHC biosensors (ForteBio) with recombinant Omicron RBDs acting as the analyte with serial dilutions. Kd values were calculated using Data Analysis HT 10 (ForteBio) with a 1:1 Langmuir binding model.

Cryo-EM sample preparation and data collection

The omicron B.1.1.529 spike trimer (Sino Biological Cat: 40589-V08H26) at a final concentration of 0.6 mg/mL was mixed with MB.02 Fab at a molar ratio of 1:1.5 on ice for 30mins. The omicron BA.5 spike trimer (ACROBiosystems SPN-C522e-50ug) at a final concentration of 0.6 mg/mL was mixed with the bispecific antibody 0213 at a molar ratio of 1:1 on ice for 30mins. Then 3 µl of the mixture was applied to a Quantifoil-Au-2/1-3C grid (Quantifoil) pretreated by glow-discharging at 20 mA for 1 min. The grid was blotted at 18 °C with 100% humidity and plunge-frozen in liquid ethane using FEI Vitrobot Mark IV (Thermo Fisher). The grids were stored in liquid nitrogen until data collection.

Images were acquired on an FEI Titan Krios electron microscope (Thermo Fisher) equipped with a Gatan K3 Summit direct detector in super-resolution mode, at a calibrated magnification of 81,000× with the physical pixel size corresponding to 1.07 Å. Detailed data collection statistics for the Fab-spike trimer complexes are shown in a supplemental table. Automated data collection was performed using SerialEM [34].

Cryo-EM data processing

A total of 5373 movie series were collected for the complex of MB.02 Fab with omicron BA.1 S trimer. A total of 2408 movie series were collected for the complex of CoV2-0213 bsAb with the omicron BA.5 S trimer. Motion correction of the micrographs was carried out using RELION [35] and contrast transfer function (CTF) estimation was calculated using CTFFIND4 [36]. Particles were picked automatically by crYOLO [37], followed by 2D and 3D classifications without imposing symmetry. The 3D classes with different S trimer conformations were then processed separately by consensus 3D refinement and CTF refinement. For each state of the complex, local masked 3D classification without image alignment was performed focusing on one Fab-RBD region and the best class of particles was selected for consensus refinement of the whole complex. For the complex of CoV2-0213 bsAb with the omicron BA.5 S trimer, repeated consensus 3D refinement and subsequent local masked 3D classification without image alignment, focusing on the up RBD with the two associated Fabs, were performed to identify the class of S trimers with both MB.02 and Clone 13A Fabs bound to the same up RBD. Subsequently, multibody refinement was performed as described above for the rigid body containing the focused region. The 3D reconstruction of the other Fab-RBD regions were obtained with the same procedure. The final resolution of each reconstruction was determined based on the Fourier shell correlation (FSC) cutoff at 0.143 between the two half maps [38]. The final map of each body was corrected for K3 detector modulation and sharpened by a negative B-factor estimated by RELION [39], and then merged in Chimera for deposition. The local resolution estimation of each cryo-EM map is calculated by RELION[35](**Fig. S3B**).

Model building and refinement

The structure of SARS-CoV-2 omicron BA.1 spike trimer (PDB 7qo7) was used as an initial model and docked into the spike trimer portion of the cryo-EM maps using Chimera [40]. The initial model of MB.02 Fab was generated by homology modeling using SWISS-MODEL [41], and then docked into the Fab portions of the cryo-EM maps using Chimera [40]. The initial models were subsequently manually rebuilt in COOT [42], followed with real space refinement in PHENIX [43]. The final models with good geometry and fit to the map were validated using the comprehensive cryo-EM validation tool implemented in PHENIX [44]. All structural figures were generated using PyMol (http://www.pymol.org/) and ChimeraX [45].

Schematic illustrations

Schematic illustrations were created with Affinity Designer.

Reporting summaries

Statistics

For all statistical analyses, confirmed that the items mentioned in NPG reporting summary are present in the figure legend, table legend, main text, or Methods section.

Standard statistical analysis

All statistical methods are described in figure legends and/or supplementary Excel tables. **Source data and statistics** were provided in a supplemental excel table.

Software and code

Data collection

ELISA data were recorded by a microplate reader (Perkin Elmer) (no version number).

Antibody binding kinetics for anti-spike mAbs were evaluated by BLI on an Octet RED96e instrument (FortéBio) at room temperature (version 12).

Flow cytometry data were collected by ThermoFisher Attune and/or BD FACS Aria flow cytometers.

Cryo-EM data were acquired on a FEI Titan Krios electron microscope (Thermo Fisher) equipped with a Gatan K3 Summit direct detector in super-resolution mode, at a calibrated magnification of 81,000× with the physical pixel size corresponding to 1.070 Å. Detailed data collection statistics for the Fab-spike trimer complexes are shown in a supplemental table. Automated data collection was performed using SerialEM (v3.8).

Data analysis

Data analysis were performed using the following software / code:

Flow data were analyzed by FlowJo v.10.7

Standard biological assays' data were analyzed in Prism (v8 or v9).

BLI data was analyzed by using Octet Analysis Studio Software 10.0.

Motion correction of the micrographs was carried out using RELION (v4.0) and contrast transfer function (CTF) estimation was calculated using CTFFIND4 (v4.1).

Particles were picked automatically by crYOLO (v1.8.1), followed by 2D and 3D classifications without imposing symmetry. The 3D classes with different S trimer conformations were then processed separately by consensus 3D refinement and CTF refinement.

The final map of each body was corrected for K3 detector modulation and sharpened by a negative B-factor estimated by RELION and then merged in Chimera for deposition.

The structure of the ectodomain of SARS-CoV-2 Omicron BA.1 spike trimer (PDB 7qo7) was used as an initial model and docked into the spike trimer portion of the cryo-EM maps using Chimera (v1.15). The initial structural model of MB.02 Fab were generated by homology modeling using SWISS-MODEL (online https://swissmodel.expasy.org), and then docked into the Fab portions of the cryo-EM maps using Chimera.

The initial models were subsequently manually rebuilt in COOT (0.9.7), followed with real-space refinement in PHENIX (v1.19).

The final models with good geometry and fit to the map were validated using the comprehensive cryo-EM validation tool implemented in PHENIX. All structural figures were generated using PyMol (v1.3) (online http://www.pymol.org/) and ChimeraX (v1.2).

Data and resource availability

All data generated or analyzed during this study are included in this article and its supplementary information files. Specifically, source data and statistics for regular experiments are provided in an excel file of **Source data and statistics**. The models of the mAb:Spike complexes have been deposited in the wwPDB with pending accession codes (1uSpike-MB.02, 8DZH; 2uSpike-MB.02, 8DZI). The cryo-EM maps of the mAb:Spike complexes have been deposited in EMDB with pending accession codes (1uSpike-MB.02, EMD-27798; 2uSpike-MB.02, EMD-27799; 1uSpike-CoV2-0213, EMD-27800). Other materials and data are available either through public repositories, or via reasonable requests to the corresponding authors to the academic community.

Code availability

No custom code was used in this study.

Life sciences study design

Sample size determination

Sample size was determined according to the lab's prior work or similar approaches in the field. For most cases, at least biological triplicate experiments (n >= 3) were performed unless otherwise noted. Details on sample size for experiments were indicated in methods and figure legends.

Data exclusions

No data were excluded.

Replication

All experiments were done with replicates. Experimental replications were indicated in detail in methods section and in each figure panel's legend. All key experiments were successful replicated in lab to ensure the rigor of the findings.

Randomization

Each sample was randomly allocated into experimental or control groups.

Blinding

The experiments were not blinded.

Reporting for specific materials, systems and methods

Antibodies used

Custom Antibodies generated in this study, where dilutions were often serial titrations (i.e. a number of dilutions as specified in each figure and/or legend.)

COV2-0208 (generated in this study)

COV2-0203 (generated in this study)

COV2-0803 (generated in this study)

COV2-0213 (generated in this study)

COV2-0813 (generated in this study)

S309 (Sotrovimab)

MB.02

MB.08

PC.03

Commercial antibodies used for staining were the following, with typical dilutions listed:

Mouse anti-Human lgGl Fc Secondary Antibody, HRP Thermo Fisher Cat#A-10648, 1:2000

InVivoMAb human lgGl isotype control BioXcell Cat#BE0297.

Goat Anti-Mouse lgG H&L (HRP) Abcam ab6789, Abcam Cat#ab6789, 1:5000.

Antibody validation

Commercial antibodies were validated by the vendors, and re-validated in house as appropriate through antigen-specific experiments. Custom antibodies were validated by specific antibody - antigen interaction assays, such as ELISA. Isotype controls were used for antibody validations.

Commercial antibody info and validation info where applicable:

https://www.thermofisher.com/antibody/product/Mouse-anti-Human-IgG1-Fc-Secondary-Antibody-clone-HP6069-Monoclonal/A-10648

https://bxcell.com/product/invivomab-human-igg1-isotype-control/

https://www.abcam.com/goat-mouse-igg-hl-hrp-ab6789.html

Eukaryotic cell lines

Cell line source(s)

All commercial cell lines were originally acquired from commercial vendors (ATCC, ThermoFisher). HEK293T (Thermo Fisher), and 293FT-hACE2 (gifted from Dr Bieniasz' lab) cell lines were used in this study.

Authentication

Cell lines were authenticated by the original commercial vendors.

Mycoplasma contamination

All the cell lines used here tested negative for mycoplasma contamination.

Commonly misidentified lines (See ICLAC register)

No commonly misidentified line was used in the study.

Flow Cytometry

Plots

Confirm the checkboxes of requirements.

Methodology

Sample preparation

Sample prep description in the Methods section.

Instrument

Flow cytometric analysis was performed on an BD FACSAria II or Thermo Attune™ NxT.

Software

FlowJo v.10.7.1 was used for flow cytometry data analysis.

Cell population abundance

N/A

Gating strategy

Cells were gated by FSC/SSC plot. To distinguish between positive and negative boundaries of the stained cells, negative control samples were analyzed and utilized as background.

Gating example figure

Confirm that a figure exemplifying the gating strategy is provided in the Supplementary Information.

Editorial Policy Items

Additional policy considerations

Macromolecular structural data

Validation report

We have provided an official validation report from wwPDB for all macromolecular structures studied.

Biological materials

Other materials and data are available either through public repositories, or via reasonable requests to the corresponding authors to the academic community.

Table 1. Cryo-EM Data Collection and Refinement Statistics

	1uSpike-MB.02 (PDB 8DZH) (EMD-27798)	2uSpike-MB.02 (PDB 8DZI) (EMD-27799)	1uSpike-CoV2-0213 (EMD-27800)
Data collection and processing			
Magnification	81000		
Voltage (kV)	300		
Electron exposure ($e^-/Å^2$)	64		64
Defocus range (μm)	-0.8 to -1.8	-0.8 to -1.8	-0.8 to -1.8
Pixel size (Å)	1.07		
Symmetry imposed	C1	C1	C1
Initial particle images (no.)	1191937		776428
Final particle images (no.)	465702	176861	26293
Map resolution (Å) FSC threshold	3.2	3.5	7.7
Refinement			
Map sharpening *B* factor ($Å^2$)	-104 to -152	-110 to -253	0
Model map FSC (masked)	0.86	0.87	
Model composition			
Non-hydrogen atoms	31967	31470	
Protein residues	3966	3918	
Ligands	73	63	
B factors ($Å^2$)			
Protein	197	234	
Ligand	212	227	
R.m.s. deviations			
Bond lengths (Å)	0.01	0.003	
Bond angles (°)	0.9	0.7	
Validation			
MolProbity score	2.1	2.0	
Clashscore	18.5	18.3	
Poor rotamers (%)	0.2	0.4	
Ramachandran plot			
Favored (%)	94.5	96.6	
Allowed (%)	5.3	3.3	
Disallowed (%)	0.2	0.2	

*1uSpike-MB.02: Omicron BA.1.1.529 Spike trimer with 2 RBDs down in complex with MB.02 Fab; 2uSpike-MB.02: Spike trimer with 1 RBD down in complex with MB.02 Fab; 1uSpike-CoV2-0213: Omicron BA.5 Spike trimer with 2 RBDs down in complex with bispecific antibody CoV2-0213.

Figure legends

Figure 1. Phylogeny, spike amino acid changes and antibody evasion of the Omicron subvariant.

A, Unrooted phylogenetic tree of Omicron and its subvariants along with other major SARS-CoV-2 variants, figure modified from the Nextstrain (https://nextstrain.org/ncov/gisaid/global/all-time), using data available from the GISAID Initiative.

B, The structure of the closed prefusion conformation of the Omicron S trimer (PDB: 7TNW) is shown in ribbon diagram with one protomer colored as NTD in orange, RBD in yellow, and the N-terminal segment of S2 in wheat. All mutations in the Omicron subvariant BA.1 and BA.2 are highlighted in sphere model.

C, Specific spike mutations found in Omicron BA.2.12.1 and Omicron BA4/BA.5 are colored compared with the sequence of Omicron BA.2 sublineage (Orange, Omicron BA.2.12.1 specific mutations; violet, Omicron BA4/BA.5 specific mutations)

D, ELISA binding curves of individual monoclonal Abs to Omicron sublineages RBD domains. The EC50 was determined by log (agonist) response of nonlinear regression and is displayed as the mean ± s.e.m.

Figure 2. Design, purification and binding assays of bsAbs to SARS-CoV-2 RBD mutants.

A, A scheme of bsAb design. Antibody domain are colored according to their architecture.

B, SDS-PAGE analysis of affinity purified bsAbs. The antibody samples are analyzed under reducing conditions (+DTT).

C, ELISA binding curves of all designed bsAbs to RBD proteins of SARS-CoV-2 WT, Delta, Omicron BA.1 and BA.2. The EC50 was determined by log (agonist) response of nonlinear regression and is displayed as the mean ± s.e.m..

D, ELISA binding curves of the lead bsAbs compared with S309 to RBD proteins of SARS-CoV-2 WA-1, Delta, Omicron BA.1 and BA.2. The EC50 was determined by log (agonist) response of nonlinear regression and is displayed as the mean ± s.e.m..

Figure 3. Neutralizing properties and binding affinity of the lead bsAbs to Omicron subvariants.

A, Neutralization potency of the lead bsAbs against pseudovirus of SARS-CoV-2 Delta and Omicron sublineages BA.1, BA.1.1 and BA.2. Serial dilutions of bsAb were added to test its neutralizing activity against indicated pseudovirus. The IC50 was determined by log (inhibitor) response of nonlinear regression and is displayed as the mean ± s.e.m..

B, Neutralization potency of remain bsAbs against pseudovirus of SARS-CoV-2 Delta and Omicron sublineages BA.1, BA.1.1 and BA.2. Serial dilutions of bsAb were added to test its neutralizing activity against indicated pseudovirus. The IC50 was determined by log (inhibitor) response of nonlinear regression and is displayed as the mean ± s.e.m..

C, Binding affinity analysis of lead bsAb CoV2-0213 to the RBD of Omicron subvariant BA.1 and BA.2. bsAbs were immobilized on AHC sensor and tested for real-time association and dissociation of the RBD (BA.1, left panel, BA.2, right panel). Global fit curves are shown as red dotted lines. The vertical dashed lines indicate the transition between association and dissociation phase.

Figure 4. Cryo-EM structures of SARS-CoV-2 Omicron BA.1 spike trimer in complex with MB.02 antibody.

A, Cryo-EM structures of MB.02 Fab fragment in complex with spike trimer in two different conformations, with one RBD up (left) or two RBDs up (right). Fab molecules are shown in different colors, and spike is shown as dark gray. The corresponding particle distribution of each spike trimer conformation is shown.

B, Overlay of the structures of human ACE2 (PDB 7wpb) and MB.02 Fab onto the same spike RBD by superimposing the RBD regions.

C, The binding conformations of the three CDRH and the three CDRL loops of MB.02 Fab on spike RBD. Upper panel, top view; lower panel, side view. The omicron BA.1.1.529 mutation N440K and G446S, which is located at the MB.02 binding interface and inserted between CDRH1 and CDRH2 loops of MB.02 Fab, is show in stick representation. The nomenclature of the top surface of spike RBD is illustrated in the middle inset.

Figure 5. Cross-reactive binding affinity of the lead bsAb CoV2-0213 to multiple Omicron subvariants.

A, ELISA binding curves of lead bsAb CoV2-0213 against SARS-CoV-2 Omicron BA.2, BA.2.12.1, BA.3 and BA.4/BA.5 RBD proteins. The EC50 was determined by log (agonist) response of nonlinear regression and is displayed as the mean ± s.e.m..

B, Binding affinity analysis of lead bsAb CoV2-0213 to the RBD of Omicron subvariant BA.2, BA.2.12.1, BA.3 and BA.4/BA.5. bsAbs were immobilized on AHC sensor and tested for real-time association and dissociation of the RBD (BA.2, left upper panel, BA.2.12.1, right upper panel, BA.3, left lower panel, BA.4/BA.5, right lower panel). Global fit curves are shown as red dotted lines. The vertical dashed lines indicate the transition between association and dissociation phase.

Figure 6. Cryo-EM reconstruction of SARS-CoV-2 Omicron BA.5 spike trimer in complex with bispecific antibody CoV2-0213 with both Fab arms engaged with RBD.

A, Overlay of the structures of the humanized clone 2 (Clone 13A) and MB.02 Fab fragments on the same spike RBD. S446 at the MB.02-bound interface of Omicron BA.1/3 spike RBD, and F486 at the Clone 13A-bound interface of WT and Omicron BA.1/2/3 spike RBD, are shown as red spheres. The nomenclature of the top surface of spike RBD is illustrated in the lower panel.

B, Cryo-EM reconstruction (left panel) and fitted models (right panel) of the CoV2-0213 antibody bound Omicron BA.5 spike trimer with one RBD up. Fab molecules are shown in different colors, and spike is shown in dark gray. The up RBD has both MB.02 and Clone 13A Fab fragments bound at distinct interfaces. The other two RBDs in down conformation has the MB.02 Fab bound. The models of the Fab variable domains (MB.02, pink; Clone 13A, blue; RBD, black) are fitted into the 3D reconstruction.

C, Cartoon illustrations of the possible bivalent binding of one CoV2-0213bsAb onto a single or two adjacent spike RBDs in the same S trimer. The Fc fragment and hinge region of the IgG are show in cartoon.

Supplemental figure legends

Figure S1. ACE2/RBD binding inhibition for the lead bsAbs.

Competition ELISA of lead bispecific Abs with human ACE2 for epitope identification to SARS-CoV-2 WT, Delta, Omicron BA.1 and BA.2 RBD proteins. The data were obtained from a representative experiment with three replicates. Data are represented as mean ± s.e.m. IC50 values were calculated from ACE2 competition ELISA assays by fitting a log (inhibitor) response of a nonlinear regression model.

Figure S2. Representative flow gating plots.

Figure S3. Local flexibility and resolution estimation of the cryo-EM reconstructions.

A, Example of one RBD-MB.02 Fab protomer that has flexible conformations.

B, Local resolution estimation of the reconstructions of MB.02 Fab in complex with Omicron BA.1 spike trimer of two different conformations.

C, Local resolution estimation of the reconstruction of bispecific antibody CoV2-0213 in complex with Omicron BA.5 spike trimer.

Source data and statistics

Source data and statistics provided in an excel file.

References

1 Acuti Martellucci, C. *et al.* SARS-CoV-2 pandemic: An overview. *Adv Biol Regul* **77**, 100736, doi:10.1016/j.jbior.2020.100736 (2020).

2 Liu, L. *et al.* Striking antibody evasion manifested by the Omicron variant of SARS-CoV-2. *Nature* **602**, 676-681, doi:10.1038/s41586-021-04388-0 (2022).

3 Planas, D. *et al.* Considerable escape of SARS-CoV-2 Omicron to antibody neutralization. *Nature* **602**, 671-675, doi:10.1038/s41586-021-04389-z (2022).

4 Rossler, A., Riepler, L., Bante, D., von Laer, D. & Kimpel, J. SARS-CoV-2 Omicron Variant Neutralization in Serum from Vaccinated and Convalescent Persons. *N Engl J Med* **386**, 698-700, doi:10.1056/NEJMc2119236 (2022).

5 Cao, Y. *et al.* Omicron escapes the majority of existing SARS-CoV-2 neutralizing antibodies. *Nature* **602**, 657-663, doi:10.1038/s41586-021-04385-3 (2022).

6 Cele, S. *et al.* Omicron extensively but incompletely escapes Pfizer BNT162b2 neutralization. *Nature* **602**, 654-656, doi:10.1038/s41586-021-04387-1 (2022).

7 Zhou, T. *et al.* Structural basis for potent antibody neutralization of SARS-CoV-2 variants including B.1.1.529. *Science*, eabn8897, doi:10.1126/science.abn8897 (2022).

8 Iketani, S. *et al.* Antibody evasion properties of SARS-CoV-2 Omicron sublineages. *Nature*, doi:10.1038/s41586-022-04594-4 (2022).

9 Yu, J. *et al.* Comparable Neutralization of the SARS-CoV-2 Omicron BA.1 and BA.2 Variants. *medRxiv*, doi:10.1101/2022.02.06.22270533 (2022).

10 Hachmann, N. P. *et al.* Neutralization Escape by SARS-CoV-2 Omicron Subvariants BA.2.12.1, BA.4, and BA.5. *N Engl J Med* **387**, 86-88, doi:10.1056/NEJMc2206576 (2022).

11 Evans, J. P. *et al.* Neutralization of the SARS-CoV-2 Deltacron and BA.3 Variants. *N Engl J Med* **386**, 2340-2342, doi:10.1056/NEJMc2205019 (2022).

12 Brown, P. E. *et al.* Omicron BA.1/1.1 SARS-CoV-2 Infection among Vaccinated Canadian Adults. *N Engl J Med* **386**, 2337-2339, doi:10.1056/NEJMc2202879 (2022).

13 Wang, Q. *et al.* Antibody evasion by SARS-CoV-2 Omicron subvariants BA.2.12.1, BA.4, & BA.5. *Nature*, doi:10.1038/s41586-022-05053-w (2022).

14 Takashita, E. *et al.* Efficacy of Antibodies and Antiviral Drugs against Omicron BA.2.12.1, BA.4, and BA.5 Subvariants. *N Engl J Med*, doi:10.1056/NEJMc2207519 (2022).

15 Tuekprakhon, A. *et al.* Antibody escape of SARS-CoV-2 Omicron BA.4 and BA.5 from vaccine and BA.1 serum. *Cell* **185**, 2422-2433 e2413, doi:10.1016/j.cell.2022.06.005 (2022).

16 Cao, Y. *et al.* BA.2.12.1, BA.4 and BA.5 escape antibodies elicited by Omicron infection. *Nature*, doi:10.1038/s41586-022-04980-y (2022).

17 Vangeel, L. *et al.* Remdesivir, Molnupiravir and Nirmatrelvir remain active against SARS-CoV-2 Omicron and other variants of concern. *Antiviral Res* **198**, 105252, doi:10.1016/j.antiviral.2022.105252 (2022).

18 P. Ren, L. P., Z. Fang, K. Suzuki, P. Renauer, Q. Lin, M. Bai, L. Yang, T. Li, P. Clark, D. Klein, S. Chen. Potent and specific human monoclonal antibodies against SARS-CoV-2 Omicron variant by rapid mRNA immunization of humanized mice. *bioRxiv* (2022).

19 Baum, A. *et al.* REGN-COV2 antibodies prevent and treat SARS-CoV-2 infection in rhesus macaques and hamsters. *Science* **370**, 1110-1115, doi:10.1126/science.abe2402 (2020).

20 Baum, A. *et al.* Antibody cocktail to SARS-CoV-2 spike protein prevents rapid mutational escape seen with individual antibodies. *Science* **369**, 1014-1018, doi:10.1126/science.abd0831 (2020).

21 Wang, N. *et al.* Structure-based development of human antibody cocktails against SARS-CoV-2. *Cell Res* **31**, 101-103, doi:10.1038/s41422-020-00446-w (2021).

22 Li, C. *et al.* Broad neutralization of SARS-CoV-2 variants by an inhalable bispecific single-domain antibody. *Cell* **185**, 1389-1401 e1318, doi:10.1016/j.cell.2022.03.009 (2022).

23 Demanet, C., Brissinck, J., De Jonge, J. & Thielemans, K. Bispecific antibody-mediated immunotherapy of the BCL1 lymphoma: increased efficacy with multiple injections and CD28-induced costimulation. *Blood* **87**, 4390-4398 (1996).

24 Li, J. F., Niu, Y. Y., Xing, Y. L. & Liu, F. A novel bispecific c-MET/CTLA-4 antibody targetting lung cancer stem cell-like cells with therapeutic potential in human non-small-cell lung cancer. *Biosci Rep* **39**, doi:10.1042/BSR20171278 (2019).

25 Xiong, M. *et al.* A Novel CD3/BCMA Bispecific T-cell Redirecting Antibody for the Treatment of Multiple Myeloma. *J Immunother* **45**, 78-88, doi:10.1097/CJI.0000000000000401 (2022).

26 Bournazos, S., Gazumyan, A., Seaman, M. S., Nussenzweig, M. C. & Ravetch, J. V. Bispecific Anti-HIV-1 Antibodies with Enhanced Breadth and Potency. *Cell* **165**, 1609-1620, doi:10.1016/j.cell.2016.04.050 (2016).

27 Frei, J. C. *et al.* Bispecific Antibody Affords Complete Post-Exposure Protection of Mice from Both Ebola (Zaire) and Sudan Viruses. *Sci Rep* **6**, 19193, doi:10.1038/srep19193 (2016).

28 Moshoette, T., Ali, S. A., Papathanasopoulos, M. A. & Killick, M. A. Engineering and characterising a novel, highly potent bispecific antibody iMab-CAP256 that targets HIV-1. *Retrovirology* **16**, 31, doi:10.1186/s12977-019-0493-y (2019).

29 Peng, L. *et al.* Monospecific and bispecific monoclonal SARS-CoV-2 neutralizing antibodies that maintain potency against B.1.617. *Nat Commun* **13**, 1638, doi:10.1038/s41467-022-29288-3 (2022).

30 Garcia-Beltran, W. F. *et al.* mRNA-based COVID-19 vaccine boosters induce neutralizing immunity against SARS-CoV-2 Omicron variant. *Cell*, doi:10.1016/j.cell.2021.12.033 (2022).

31 Bewley, K. R. *et al.* Quantification of SARS-CoV-2 neutralizing antibody by wild-type plaque reduction neutralization, microneutralization and pseudotyped virus neutralization assays. *Nat Protoc* **16**, 3114-3140, doi:10.1038/s41596-021-00536-y (2021).

32 Nie, J. *et al.* Quantification of SARS-CoV-2 neutralizing antibody by a pseudotyped virus-based assay. *Nat Protoc* **15**, 3699-3715, doi:10.1038/s41596-020-0394-5 (2020).

33 Liu, L. *et al.* Potent neutralizing antibodies against multiple epitopes on SARS-CoV-2 spike. *Nature* **584**, 450-456, doi:10.1038/s41586-020-2571-7 (2020).

34 Mastronarde, D. N. Automated electron microscope tomography using robust prediction of specimen movements. *J Struct Biol* **152**, 36-51, doi:10.1016/j.jsb.2005.07.007 (2005).

35 Kimanius, D., Dong, L., Sharov, G., Nakane, T. & Scheres, S. H. W. New tools for automated cryo-EM single-particle analysis in RELION-4.0. *Biochem J* **478**, 4169-4185, doi:10.1042/BCJ20210708 (2021).

36 Rohou, A. & Grigorieff, N. CTFFIND4: Fast and accurate defocus estimation from electron micrographs. *J Struct Biol* **192**, 216-221, doi:10.1016/j.jsb.2015.08.008 (2015).

37 Wagner, T. *et al.* SPHIRE-crYOLO is a fast and accurate fully automated particle picker for cryo-EM. *Commun Biol* **2**, 218, doi:10.1038/s42003-019-0437-z (2019).

38 Scheres, S. H. & Chen, S. Prevention of overfitting in cryo-EM structure determination. *Nat Methods* **9**, 853-854, doi:10.1038/nmeth.2115 (2012).

39 Rosenthal, P. B. & Henderson, R. Optimal determination of particle orientation, absolute hand, and contrast loss in single-particle electron cryomicroscopy. *J Mol Biol* **333**, 721-745, doi:10.1016/j.jmb.2003.07.013 (2003).

40 Pettersen, E. F. *et al.* UCSF Chimera--a visualization system for exploratory research and analysis. *J Comput Chem* **25**, 1605-1612, doi:10.1002/jcc.20084 (2004).

41 Waterhouse, A. *et al.* SWISS-MODEL: homology modelling of protein structures and complexes. *Nucleic Acids Res* **46**, W296-W303, doi:10.1093/nar/gky427 (2018).

42 Emsley, P., Lohkamp, B., Scott, W. G. & Cowtan, K. Features and development of Coot. *Acta Crystallogr D Biol Crystallogr* **66**, 486-501, doi:10.1107/S0907444910007493 (2010).

43 Afonine, P. V. *et al.* Real-space refinement in PHENIX for cryo-EM and crystallography. *Acta Crystallogr D Struct Biol* **74**, 531-544, doi:10.1107/S2059798318006551 (2018).

44 Afonine, P. V. *et al.* New tools for the analysis and validation of cryo-EM maps and atomic

models. *Acta Crystallogr D Struct Biol* **74**, 814-840, doi:10.1107/S2059798318009324 (2018).

45 Pettersen, E. F. *et al.* UCSF ChimeraX: Structure visualization for researchers, educators, and developers. *Protein Sci* **30**, 70-82, doi:10.1002/pro.3943 (2021).

Figure 1

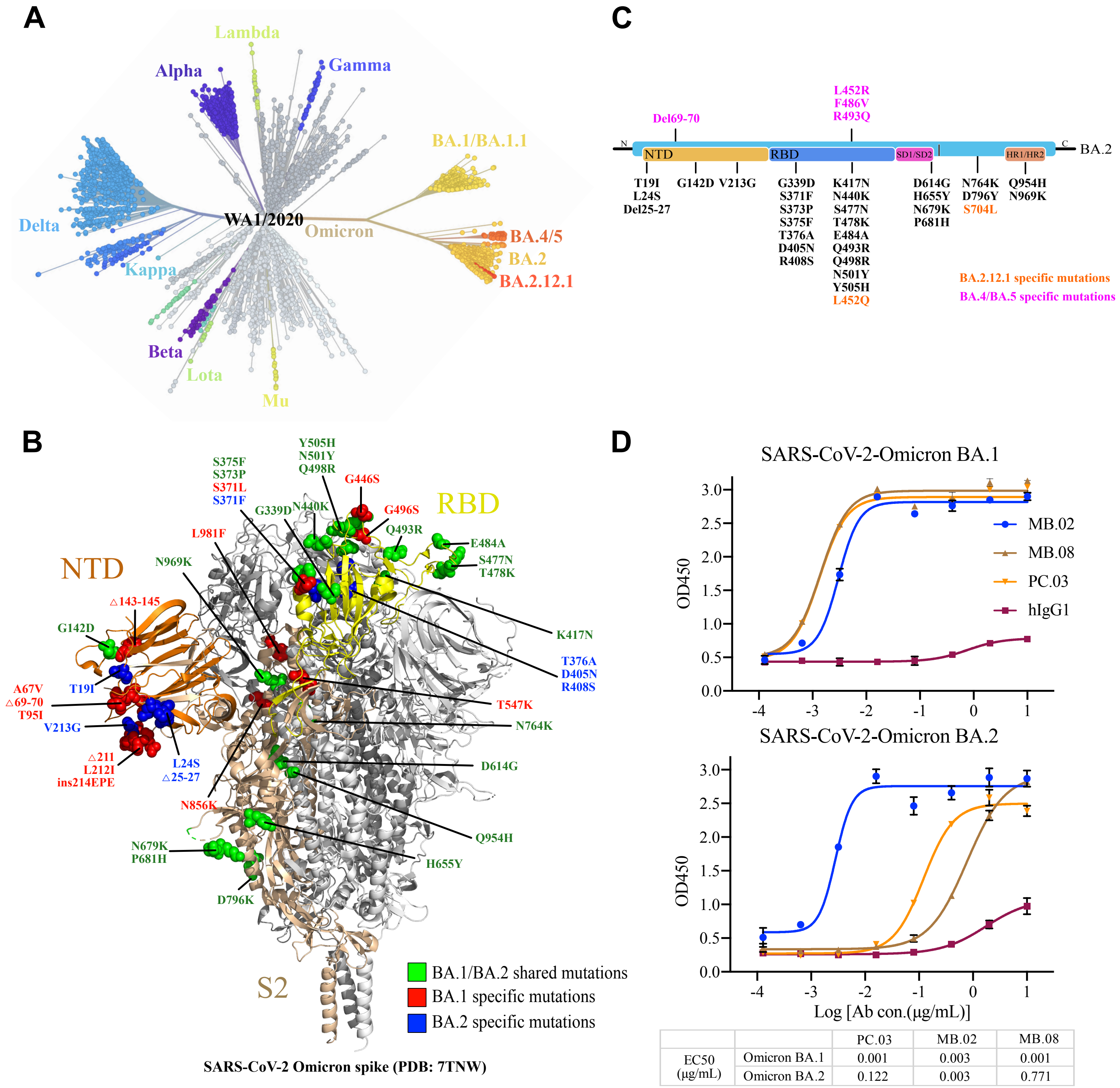

		PC.03	MB.02	MB.08
EC50 (μg/mL)	Omicron BA.1	0.001	0.003	0.001
	Omicron BA.2	0.122	0.003	0.771

Figure 2

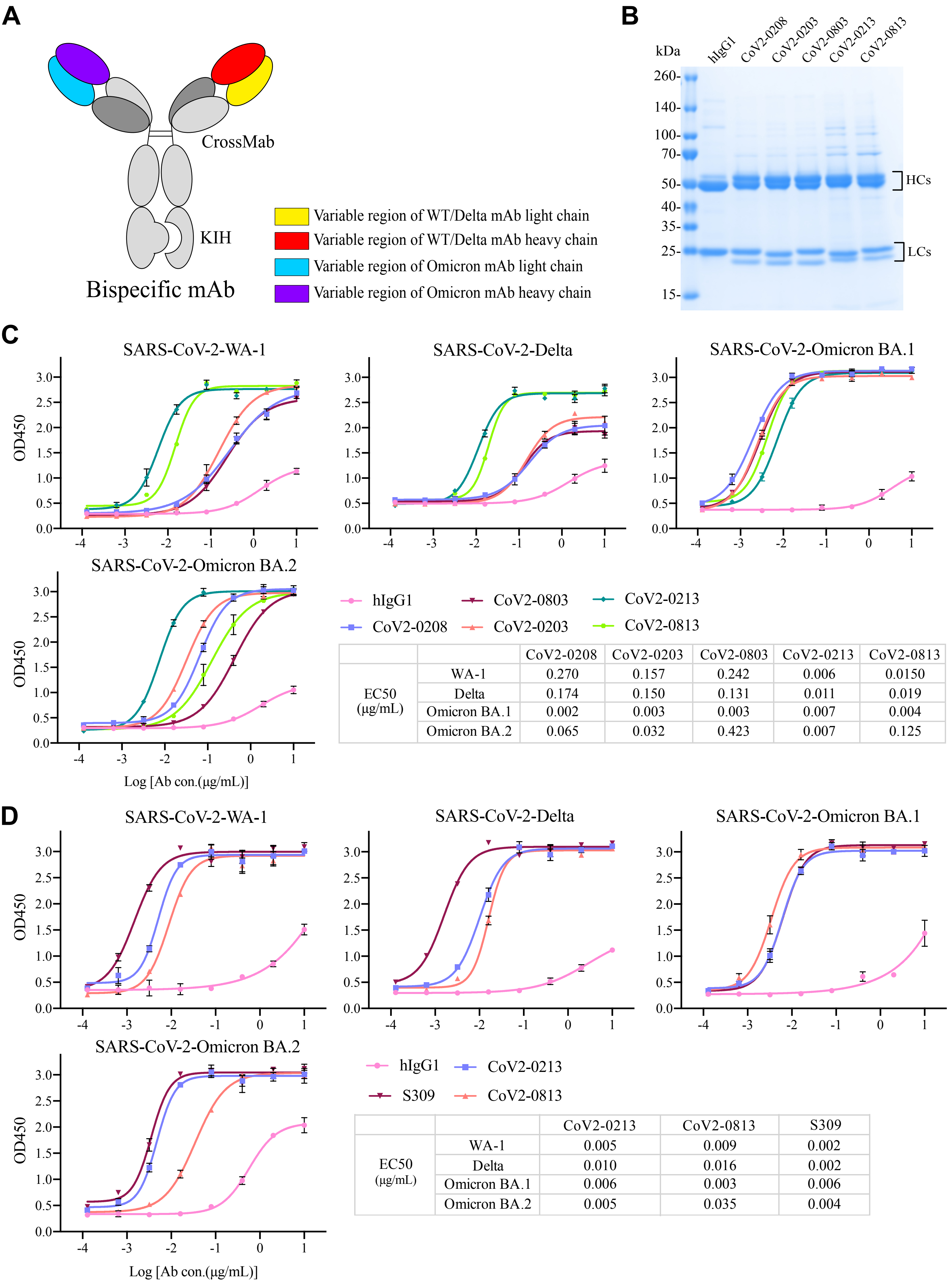

		CoV2-0208	CoV2-0203	CoV2-0803	CoV2-0213	CoV2-0813
EC50 (μg/mL)	WA-1	0.270	0.157	0.242	0.006	0.0150
	Delta	0.174	0.150	0.131	0.011	0.019
	Omicron BA.1	0.002	0.003	0.003	0.007	0.004
	Omicron BA.2	0.065	0.032	0.423	0.007	0.125

		CoV2-0213	CoV2-0813	S309
EC50 (μg/mL)	WA-1	0.005	0.009	0.002
	Delta	0.010	0.016	0.002
	Omicron BA.1	0.006	0.003	0.006
	Omicron BA.2	0.005	0.035	0.004

Figure 3

A

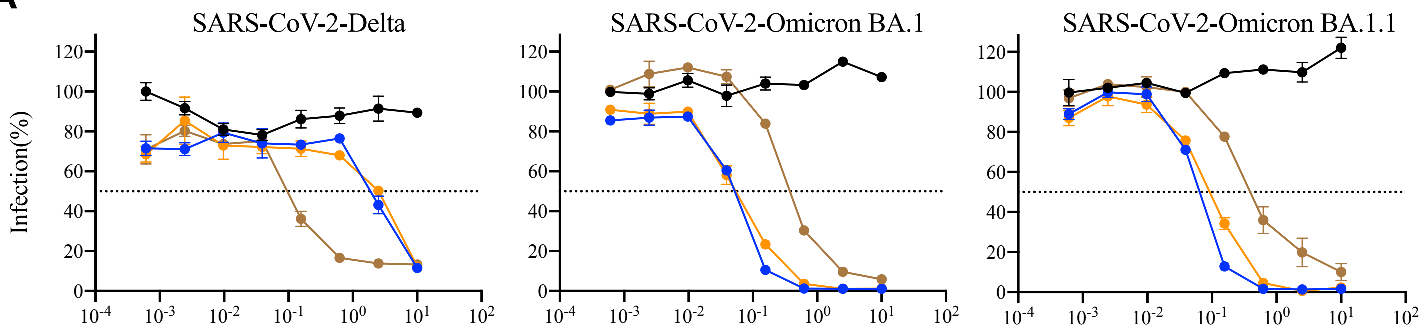

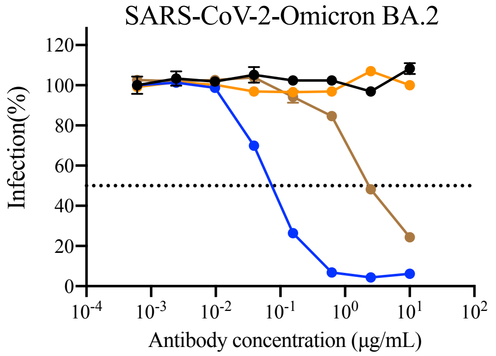

		CoV2-0213	CoV2-0813	S309
IC50 (μg/mL)	Delta	1.555	1.482	0.091
	Omicron BA.1	0.044	0.053	0.446
	Omicron BA.1.1	0.062	0.091	0.533
	Omicron BA.2	0.078	N/A	2.747

B

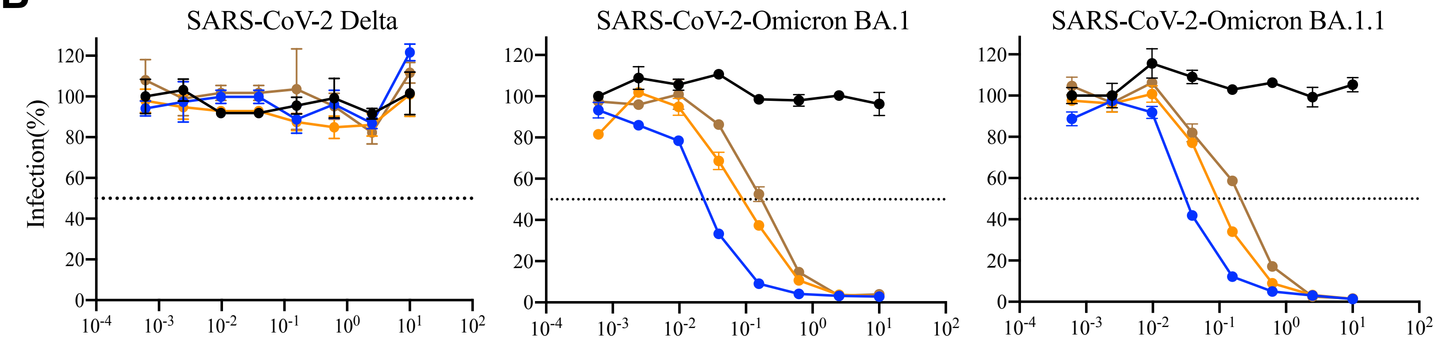

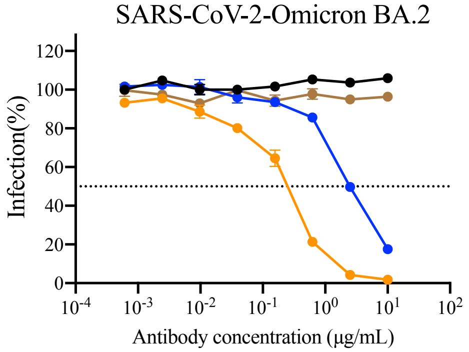

		CoV2-0208	CoV2-0203	CoV2-0803
IC50 (μg/mL)	Delta	N/A	N/A	N/A
	Omicron BA.1	0.023	0.091	0.169
	Omicron BA.1.1	0.035	0.101	0.188
	Omicron BA.2	2.584	0.210	N/A

C

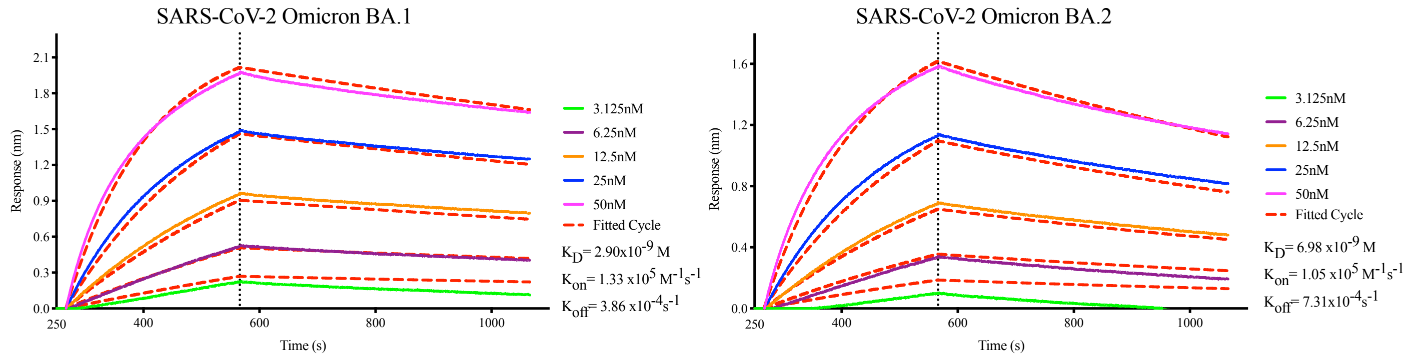

Figure 4

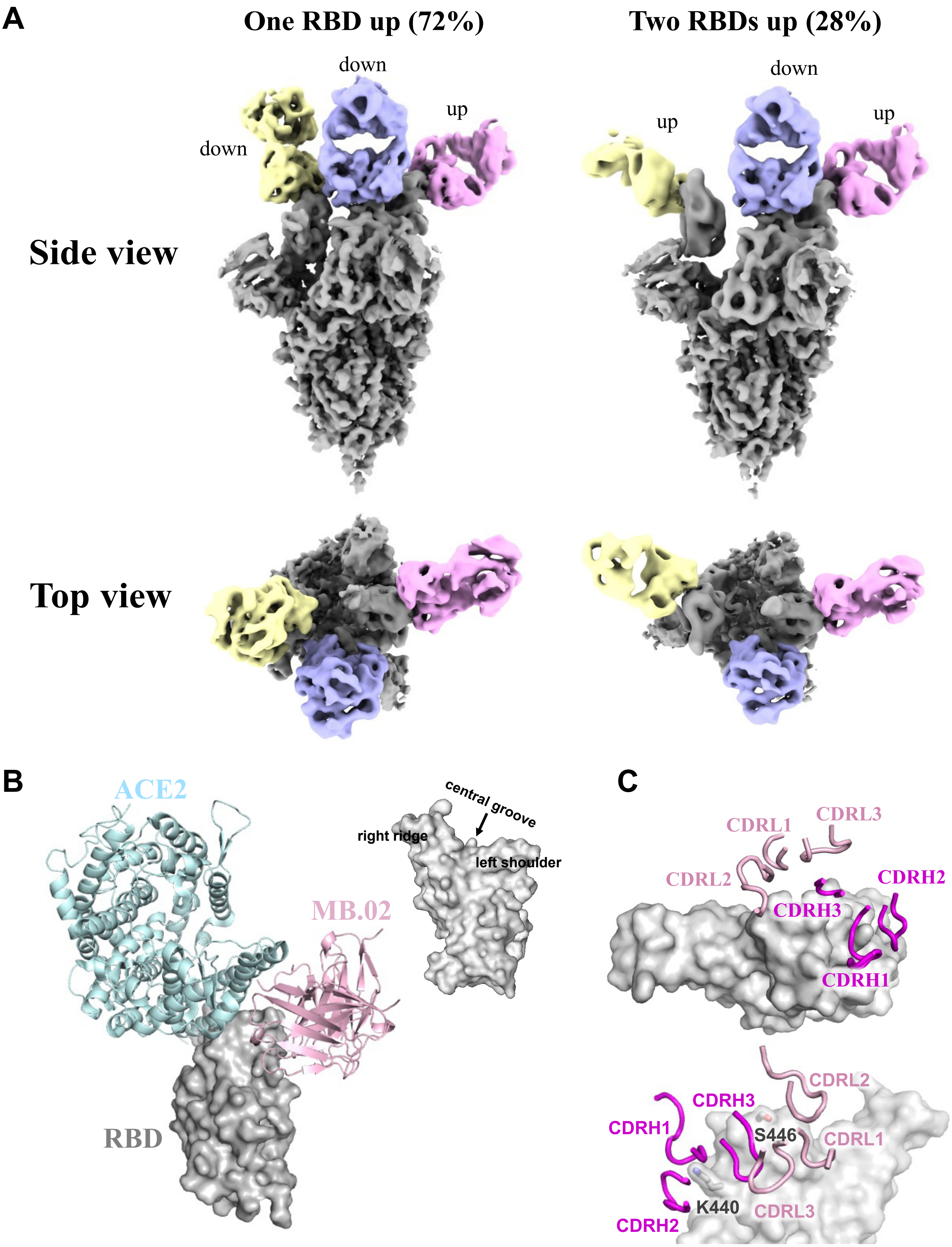
A
One RBD up (72%)
Two RBDs up (28%)
down
up
down
down
up
up
Side view
Top view
B
ACE2
MB.02
RBD
central groove
right ridge
left shoulder
C
CDRL1
CDRL3
CDRL2
CDRH2
CDRH3
CDRH1
CDRL2
CDRH3
CDRH1
S446
CDRL1
K440
CDRL3
CDRH2

Figure 5

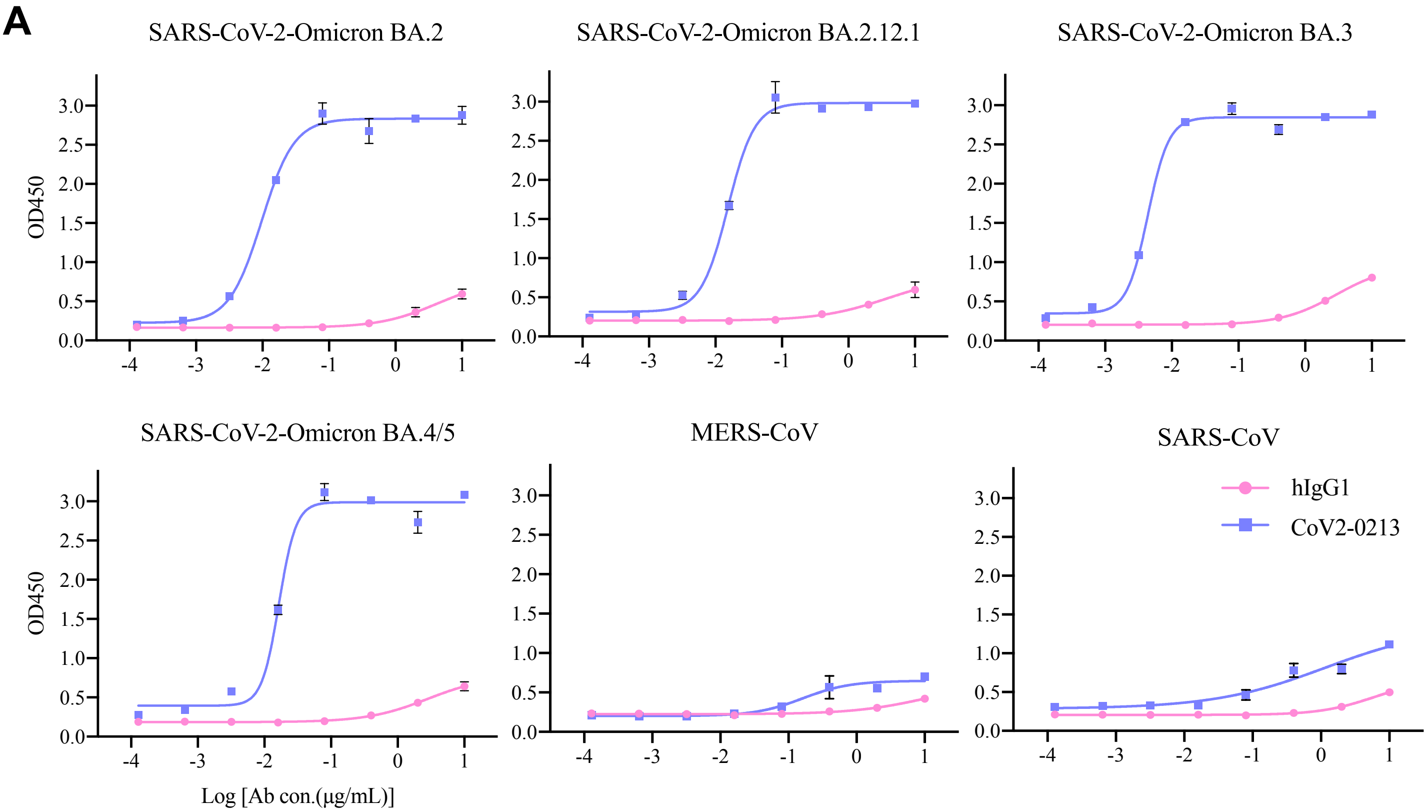

		Omicron BA.2	Omicron BA.2.12.1	Omicron BA.3	Omicron BA.4/BA.5	MERS-CoV	SARS-CoV
EC50 (μg/mL)	CoV2-0213	0.0097	0.0154	0.0044	0.0165	N/A	N/A

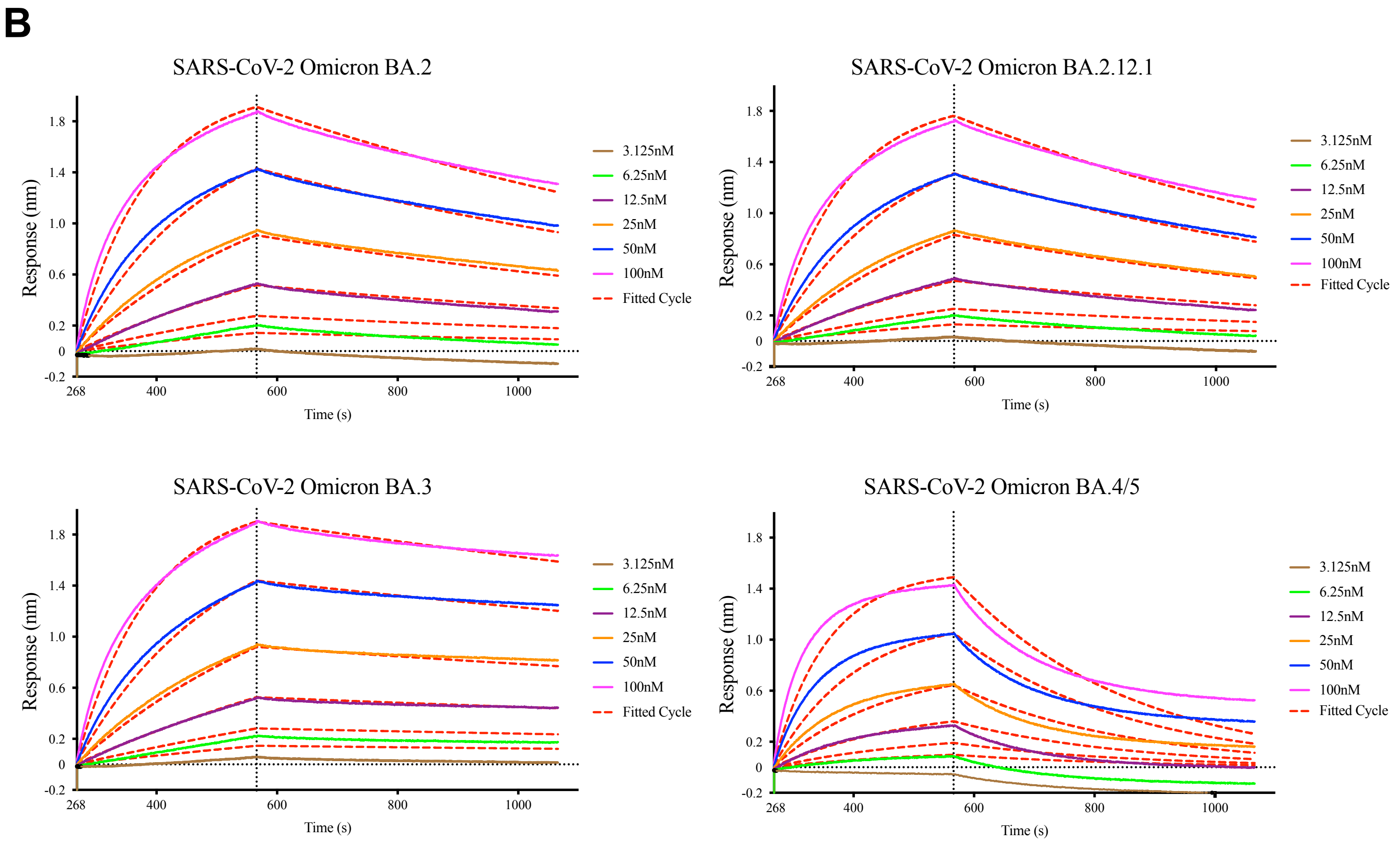

Figure 6

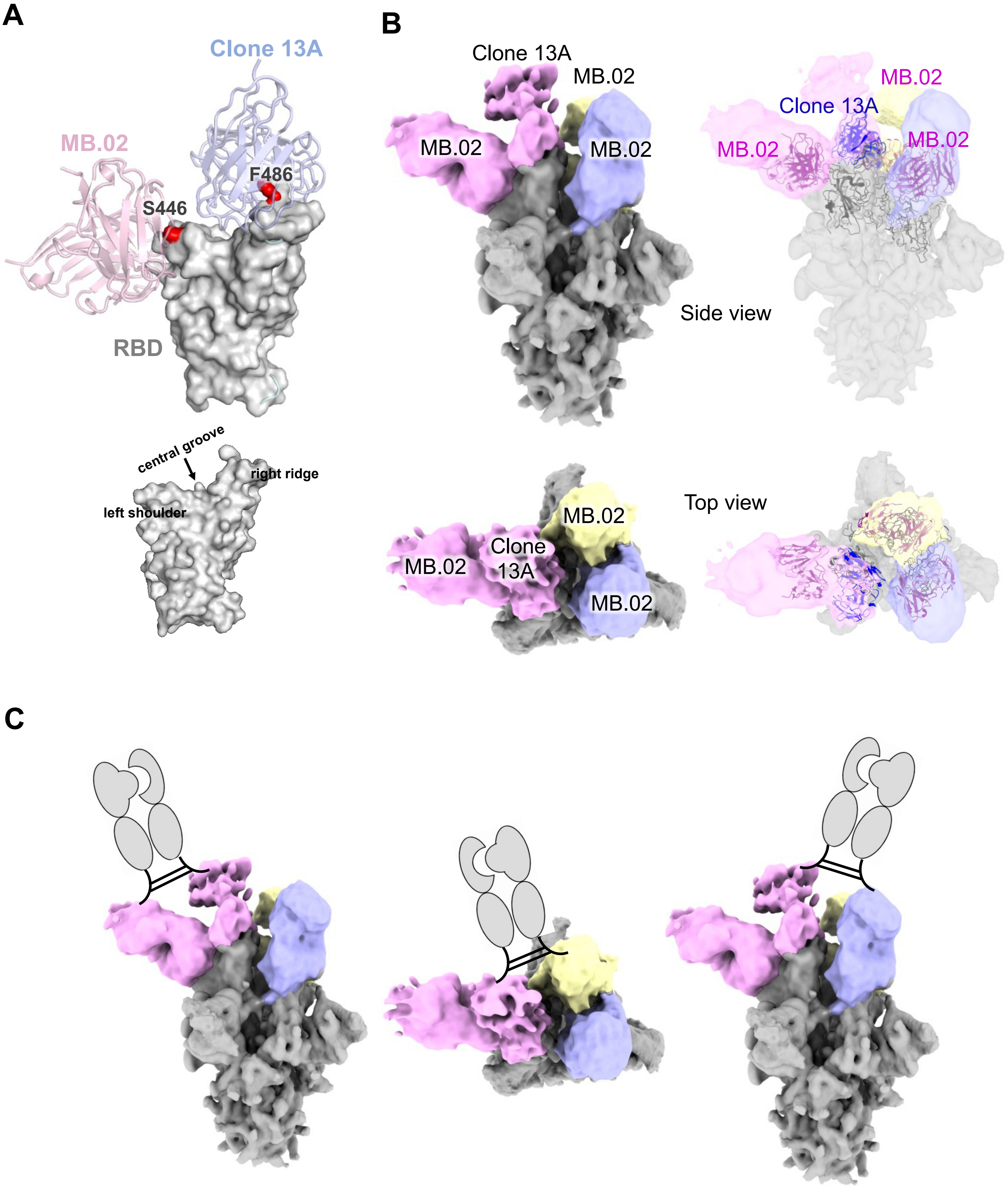
A
Clone 13A
MB.02
F486
S446
RBD
central groove
right ridge
left shoulder
B
Clone 13A
MB.02
MB.02
MB.02
MB.02
Clone 13A
MB.02
MB.02
Side view
Top view
MB.02
Clone
13A
MB.02
MB.02
C

Figure S1

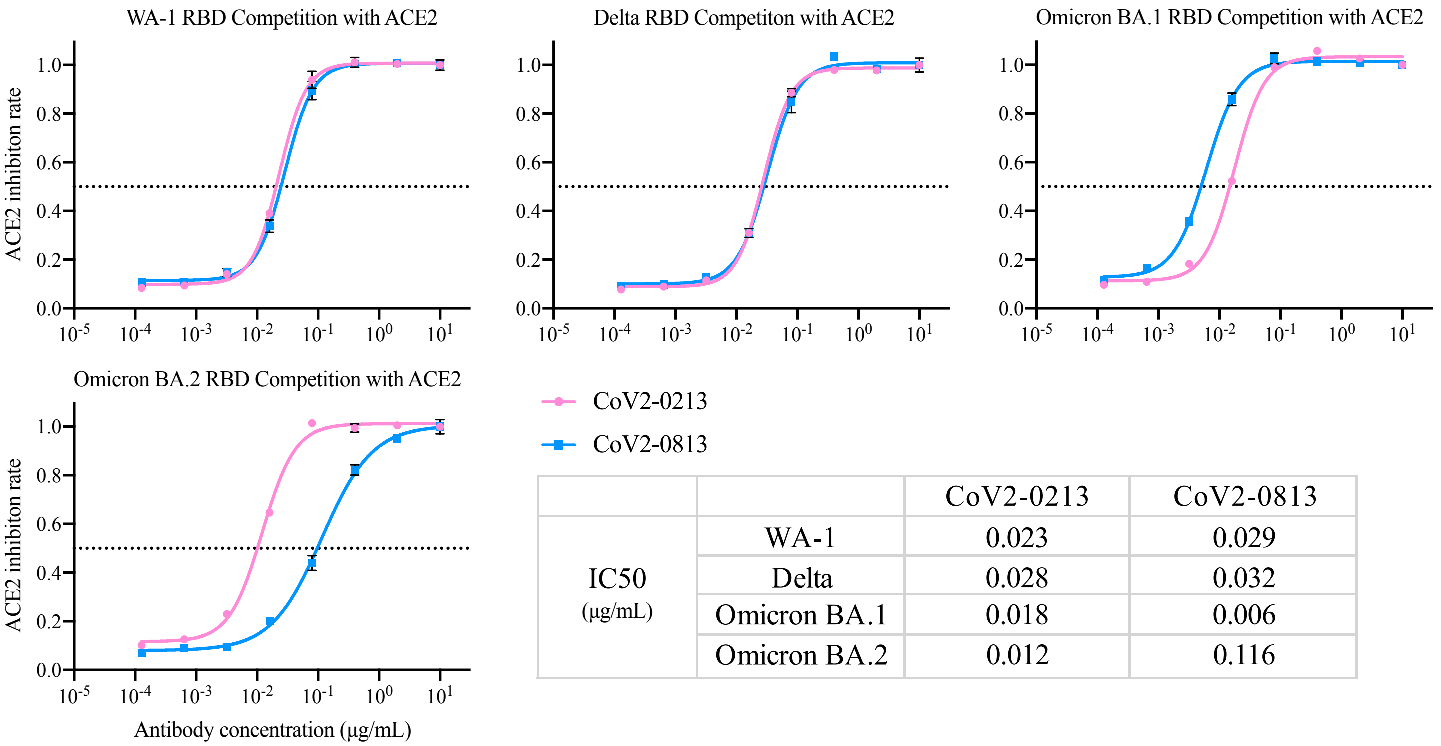

		CoV2-0213	CoV2-0813
IC50 (μg/mL)	WA-1	0.023	0.029
	Delta	0.028	0.032
	Omicron BA.1	0.018	0.006
	Omicron BA.2	0.012	0.116

Figure S2

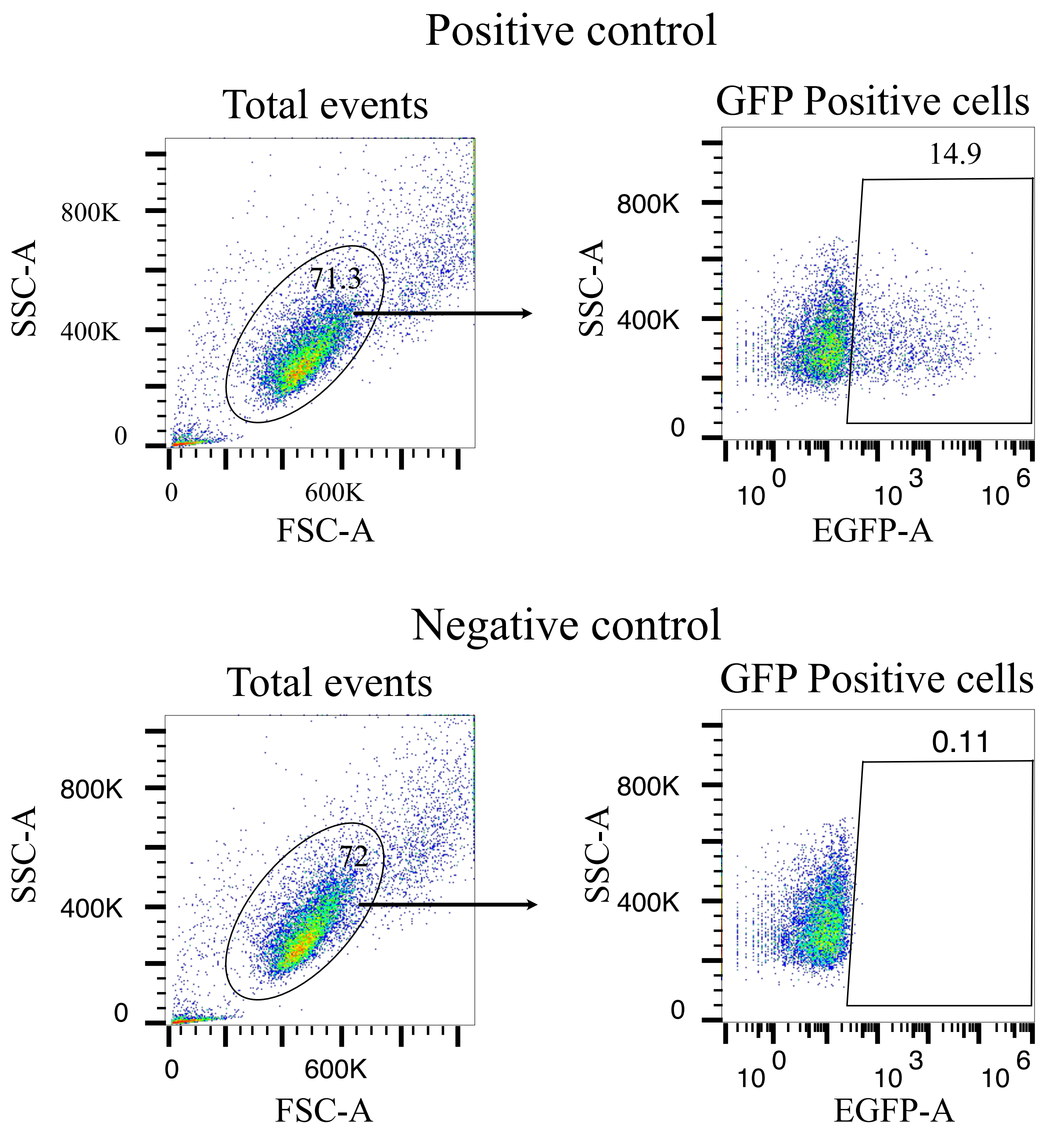
Positive control
Total events
SSC-A
800K
400K
0
71.3
0
600K
FSC-A
GFP Positive cells
SSC-A
800K
400K
0
14.9
10 0
10 3
10 6
EGFP-A
Negative control
Total events
SSC-A
800K
400K
0
72
0
600K
FSC-A
GFP Positive cells
SSC-A
800K
400K
0
0.11
10 0
10 3
10 6
EGFP-A

Figure S3